Research Article | Vol. 7, No. 3 | 1 Mar 2017 | OPTICAL MATERIALS EXPRESS 844

Optical Materials EXPRESS

Comparative spectroscopic and thermo-optic study of Tm:Li*Ln*F_4 (*Ln* = Y, Gd, and Lu) crystals for highly-efficient microchip lasers at ~2 μm

PAVEL LOIKO,[1,2] JOSEP MARIA SERRES,[1] XAVIER MATEOS,[1,3,6,*] SIMONE TACCHINI,[3] MAURO TONELLI,[4] STEFANO VERONESI,[4] DANIELA PARISI,[4] ALBERTO DI LIETO,[4] KONSTANTIN YUMASHEV,[5] UWE GRIEBNER,[3] AND VALENTIN PETROV[3]

[1]*Física i Cristal·lografia de Materials i Nanomaterials (FiCMA-FiCNA), Universitat Rovira i Virgili (URV), Campus Sescelades, c/ Marcel·lí Domingo, s/n., E-43007 Tarragona, Spain*
[2]*ITMO University, 49 Kronverkskiy pr., 197101 St. Petersburg, Russia*
[3]*Max Born Institute for Nonlinear Optics and Short Pulse Spectroscopy, Max-Born-Str. 2a, D-12489 Berlin, Germany*
[4]*NEST Istituto Nanoscienze-CNR and Dipartimento di Fisica dell'Università di Pisa, Largo B. Pontecorvo 3, 56127 Pisa, Italy*
[5]*Center for Optical Materials and Technologies (COMT), Belarusian National Technical University, 65/17 Nezavisimosti Ave., 220013 Minsk, Belarus*
[6]*mateos@mbi-berlin.de*
[*]*xavier.mateos@urv.cat*

Abstract: We report on a detailed comparative study of the spectroscopic and thermo-optic properties of tetragonal Tm:Li*Ln*F_4 (*Ln* = Y, Gd, and Lu) crystals indicating their suitability for highly-efficient microchip lasers diode-pumped at ~791 nm and operating at ~1.91 μm. An ***a***-cut 8 at.% Tm:$LiYF_4$ micro-laser generated 3.1 W of linearly polarized output at 1904 nm with a slope efficiency of η = 72% and a laser threshold of only 0.24 W. The internal loss for this crystal is as low as 0.0011 cm^{-1}. For 8 at.% Tm:$LiGdF_4$ and 12 at.% Tm:$LiLuF_4$ lasers, the output power reached ~2 W and η was 65% and 52%, respectively. The thermal lens in all Tm:Li*Ln*F_4 crystals is weak, positive and low-astigmatic. The potential for the Tm:Li*Ln*F_4 lasers to operate beyond ~2 μm due to a vibronic coupling has been proved. The Tm:$LiYF_4$ vibronic laser generated 375 mW at 2026-2044 nm with η = 31%. The Tm:Li*Ln*F_4 crystals are very promising for passively Q-switched microchip lasers.

OCIS codes: (140.3380) Laser materials; (300.0300) Spectroscopy; (140.3480) Lasers, diode-pumped.

References and links

1. S. So, J. I. Mackenzie, D. P. Sheperd, W. A. Clarkson, J. G. Betterton, and E. K. Gorton, "A power-scaling strategy for longitudinally diode-pumped Tm:YLF lasers," Appl. Phys. B **84**(3), 389–393 (2006).
2. M. Schellhorn, "High-power diode-pumped Tm:YLF laser," Appl. Phys. B **91**(1), 71–74 (2008).
3. X. M. Duan, B. Q. Yao, C. W. Song, J. Gao, and Y. Z. Wang, "Room temperature efficient continuous wave and Q-switched Ho:YAG laser double-pass pumped by a diode-pumped Tm:YLF laser," Laser Phys. Lett. **5**(11), 800–803 (2008).
4. M. Pollnau, P. J. Hardman, M. A. Kern, W. A. Clarkson, and D. C. Hanna, "Upconversion-induced heat generation and thermal lensing in Nd:YLF and Nd:YAG," Phys. Rev. B **58**(24), 16076–16092 (1998).
5. B. M. Walsh, N. P. Barnes, M. Petros, J. Yu, and U. N. Singh, "Spectroscopy and modeling of solid state lanthanide lasers: Application to trivalent Tm^{3+} and Ho^{3+} in $YLiF_4$ and $LuLiF_4$," J. Appl. Phys. **95**(7), 3255–3271 (2004).
6. R. Faoro, M. Kadankov, D. Parisi, S. Veronesi, M. Tonelli, V. Petrov, U. Griebner, M. Segura, and X. Mateos, "Passively Q-switched Tm:YLF laser," Opt. Lett. **37**(9), 1517–1519 (2012).
7. C. Pfistner, R. Weber, H. P. Weber, S. Merazzi, and R. Gruber, "Thermal beam distortions in end-pumped Nd: YAG, Nd:GSGG, and Nd:YLF rods," IEEE J. Quantum Electron. **30**(7), 1605–1615 (1994).
8. N. Coluccelli, G. Galzerano, F. Cornacchia, A. Di Lieto, M. Tonelli, and P. Laporta, "High-efficiency diode-pumped Tm:GdLiF4 laser at 1.9 microm," Opt. Lett. **34**(22), 3559–3561 (2009).
9. N. Coluccelli, G. Galzerano, P. Laporta, F. Cornacchia, D. Parisi, and M. Tonelli, "Tm-doped LiLuF4 crystal for efficient laser action in the wavelength range from 1.82 to 2.06 microm," Opt. Lett. **32**(14), 2040–2042 (2007).

#282975 https://doi.org/10.1364/OME.7.000844
Journal © 2017 Received 16 Dec 2016; revised 28 Jan 2017; accepted 7 Feb 2017; published 13 Feb 2017

Optical Materials EXPRESS

10. B. Oreshkov, S. Veronesi, M. Tonelli, A. di Lieto, V. Petrov, U. Griebner, X. Mateos, and I. Buchvarov, "Tm^{3+}:$LiGdF_4$ Laser, passively Q-switched with a Cr^{2+}:ZnSe saturable absorber," IEEE Photonics J. **7**(3), 1502206 (2015).
11. H. Yu, V. Petrov, U. Griebner, D. Parisi, S. Veronesi, and M. Tonelli, "Compact passively Q-switched diode-pumped Tm:$LiLuF_4$ laser with 1.26 mJ output energy," Opt. Lett. **37**(13), 2544–2546 (2012).
12. J. J. Zayhowski, "Microchip lasers," Opt. Mater. **11**(2–3), 255–267 (1999).
13. J. J. Zayhowski and C. Dill Iii, "Diode-pumped passively Q-switched picosecond microchip lasers," Opt. Lett. **19**(18), 1427–1429 (1994).
14. J. M. Serres, X. Mateos, P. Loiko, K. Yumashev, N. Kuleshov, V. Petrov, U. Griebner, M. Aguiló, and F. Díaz, "Diode-pumped microchip Tm:$KLu(WO_4)_2$ laser with more than 3 W of output power," Opt. Lett. **39**(14), 4247–4250 (2014).
15. M. Gaponenko, N. Kuleshov, and T. Südmeyer, "Passively Q-switched thulium microchip laser," IEEE Photonics Technol. Lett. **28**(2), 147–150 (2016).
16. P. Loiko, J. M. Serres, X. Mateos, K. Yumashev, A. Yasukevich, V. Petrov, U. Griebner, M. Aguiló, and F. Díaz, "Subnanosecond Tm:KLuW microchip laser Q-switched by a Cr:ZnS saturable absorber," Opt. Lett. **40**(22), 5220–5223 (2015).
17. P. Loiko, J. M. Serres, X. Mateos, H. Yu, H. Zhang, J. Liu, K. Yumashev, U. Griebner, V. Petrov, M. Aguiló, and F. Díaz, "Thermal lensing and multi-watt microchip laser operation of Yb:YCOB crystals," IEEE Photonics J. **8**(3), 1501312 (2016).
18. N. Hodgson and H. Weber, *Optical Resonators: Fundamentals, Advanced Concepts and Applications* (Springer, 1997).
19. B. F. Aull and H. P. Jenssen, "Vibronic interactions in Nd:YAG resulting in nonreciprocity of absorption and stimulated emission cross sections," IEEE J. Quantum Electron. **18**(5), 925–930 (1982).
20. S. A. Payne, L. L. Chase, L. K. Smith, W. L. Kway, and W. F. Krupke, "Infrared cross-section measurements for crystals doped with Er^{3+}, Tm^{3+}, and Ho^{3+}," IEEE J. Quantum Electron. **28**(11), 2619–2630 (1992).
21. M. Eichhorn, "Quasi-three-level solid-state lasers in the near and mid infrared based on trivalent rare earth ions," Appl. Phys. B **93**(2–3), 269–316 (2008).
22. R. L. Aggarwal, D. J. Ripin, J. R. Ochoa, and T. Y. Fan, "Measurement of thermo-optic properties of $Y_3Al_5O_{12}$, $Lu_3Al_5O_{12}$, $YAlO_3$, $LiYF_4$, $LiLuF_4$, BaY_2F_8, $KGd(WO_4)_2$, and $KY(WO_4)_2$ laser crystals in the 80–300 K temperature range," J. Appl. Phys. **98**(10), 103514 (2005).
23. K. Yumashev and P. Loiko, "Thermal stresses and end-bulging in the laser disc from a tetragonal crystal: The case of $LiYF_4$," Laser Phys. **25**(6), 065004 (2015).
24. F. Cornacchia, D. Parisi, C. Bernardini, A. Toncelli, and M. Tonelli, "Efficient, diode-pumped $Tm^{(3)+}$:$BaY_{(2)}F_{(8)}$ vibronic laser," Opt. Express **12**(9), 1982–1989 (2004).
25. P. Loiko, J. M. Serres, X. Mateos, K. Yumashev, N. Kuleshov, V. Petrov, U. Griebner, M. Aguiló, and F. Díaz, "Microchip laser operation of Tm,Ho:$KLu(WO_4)_2$ crystal," Opt. Express **22**(23), 27976–27984 (2014).
26. X. Zhang, Y. Wang, L. Li, Y. Ju, and Y. Peng, "The effects of energy transfer upconversion on end-pumped Q-switched Tm,Ho:YLF lasers," J. Phys. D Appl. Phys. **42**(2), 025107 (2009).
27. P. Loiko, X. Mateos, S. Y. Choi, F. Rotermund, J. M. Serres, M. Aguiló, F. Díaz, K. Yumashev, U. Griebner, and V. Petrov, "Vibronic thulium laser at 2131 nm Q-switched by single-walled carbon nanotubes," J. Opt. Soc. Am. B **33**(11), D19–D27 (2016).
28. M. Dulick, G. E. Faulkner, N. J. Cockroft, and D. C. Nguyen, "Spectroscopy and dynamics of upconversion in Tm^{3+}:$YLiF_4$," J. Lumin. **48–49**, 517–521 (1991).
29. S. A. Miller, H. E. Rast, and H. H. Caspers, "Lattice vibrations of $LiYF_4$," J. Chem. Phys. **52**(8), 4172–4175 (1970).
30. P. Loiko, F. Druon, P. Georges, B. Viana, and K. Yumashev, "Thermo-optic characterization of Yb:$CaGdAlO_4$ laser crystal," Opt. Mater. Express **4**(11), 2241–2249 (2014).
31. K. V. Yumashev, A. N. Zakharova, and P. A. Loiko, "Photo-elastic effect, thermal lensing and depolarization in ***a***-cut tetragonal laser crystals," Laser Phys. **26**(6), 065002 (2016).
32. P. A. Loiko, K. V. Yumashev, V. N. Matrosov, and N. V. Kuleshov, "Dispersion and anisotropy of thermo-optic coefficients in tetragonal $GdVO_4$ and YVO_4 laser host crystals," Appl. Opt. **52**(4), 698–705 (2013).
33. K. van Dalfsen, S. Aravazhi, C. Grivas, S. M. García-Blanco, and M. Pollnau, "Thulium channel waveguide laser with 1.6 W of output power and ~80% slope efficiency," Opt. Lett. **39**(15), 4380–4383 (2014).
34. J. A. Caird, S. A. Payne, P. R. Staber, A. J. Ramponi, L. L. Chase, and W. F. Krupke, "Quantum electronic properties of the $Na_3Ga_2Li_3F_{12}$:Cr^{3+} laser," IEEE J. Quantum Electron. **24**(6), 1077–1099 (1988).
35. T. Yokozawa, J. Izawa, and H. Hara, "Mode control of a Tm:YLF microchip laser by a multiple resonator," Opt. Commun. **145**(1–6), 98–100 (1998).
36. G. L. Bourdet and G. Lescroart, "Theoretical modeling and design of a Tm, Ho:$YLiF_4$ microchip laser," Appl. Opt. **38**(15), 3275–3281 (1999).
37. F. Druon, S. Ricaud, D. N. Papadopoulos, A. Pellegrina, P. Camy, J. L. Doualan, R. Moncorgé, A. Courjaud, E. Mottay, and P. Georges, "On Yb:CaF_2 and Yb:SrF_2: review of spectroscopic and thermal properties and their impact on femtosecond and high power laser performance," Opt. Mater. Express **1**(3), 489–502 (2011).

1. Introduction

The tetragonal lithium yttrium fluoride, $LiYF_4$ (shortly YLF), is a well-known crystalline laser host for trivalent lanthanide ions. Nowadays, it is widely used in efficient and power-

Optical Materials EXPRESS

scalable continuous-wave (CW) and passively Q-switched (PQS) lasers emitting at ~1 μm (Nd:YLF) and ~1.9 μm (Tm:YLF) [1,2]. The Tm:YLF lasers based on the $^3F_4 \rightarrow {}^3H_6$ transition of the Tm^{3+} ion are used in laser surgery and for pumping of high-power or high-energy Ho-doped oscillators [3]. Tm:YLF has several advantages. First, the host matrix, YLF, possesses relatively high thermal conductivity, ~6 W/(m·K) [4] which is of high relevance for power scaling. Second, from the spectroscopic point of view, it permits relatively high Tm doping levels (3–8 at.% or $N_{Tm} = 4–11 \times 10^{20}$ cm^{-3}) providing efficient cross-relaxation (CR) for the adjacent Tm^{3+} ions ($^3H_4(Tm_1) + {}^3H_6(Tm_2) \rightarrow {}^3F_4(Tm_1) + {}^3F_4\ (Tm_2)$) [1] leading to a quantum efficiency of ~2 and, consequently, to high laser efficiency. It is characterized by a very long Tm^{3+} upper-laser-level lifetime (~16 ms) [5] leading to low laser threshold in CW and to high pulse energies achievable in the PQS regime, e.g. 0.9 mJ were generated in [6] with a pulse duration of 14 ns at ~1.9 μm using using a Cr^{2+}:ZnS saturable absorber (SA). Third, Tm:YLF exhibits natural birefringence and anisotropy of the transition cross-sections [5] which eliminates the depolarization loss and provides a natural selection of the linear laser polarization. Fourth, YLF like most of the fluorides exhibits negative thermo-optic coefficient, dn/dT, which leads to weak thermal lens for certain crystal orientations [4,7]. Finally, Tm:YLF can be efficiently pumped by commercial AlGaAs laser diodes emitting at ~791 nm (into the $^3H_6 \rightarrow {}^3H_4$ band of Tm^{3+}) [1].

There exist two other fluorides isostructural to YLF. These are $LiGdF_4$ and $LiLuF_4$ (shortly GLF and LLF, respectively) [8,9] which have attracted a lot of attention in recent years for the design of PQS Tm lasers. Again due to the long storage time of the $^3F_4$ upper laser level, these crystals generated 0.47 mJ/13 ns (Tm:GLF) and 1.26 mJ/7.6 ns (Tm:LLF) pulses at ~1.9 μm, with Cr^{2+}:ZnS and Cr^{2+}:ZnSe SAs, respectively [10,11]. Such laser sources are of practical importance for medicine and sensing of CO_2 and water in the atmosphere.

The microchip laser concept implies the gain material and (optionally) a SA placed in a compact low-loss plano-plano cavity [12,13]. As for Tm lasers, and, in particular, Tm:YLF, it is known that the upconversion mechanism is a key factor limiting the laser performance for high doping levels [1]. The application of the microchip concept can partially mitigate this drawback by keeping low intracavity losses and, hence, a low inversion level in the active medium, thus fully exploiting the advantages of highly Tm-doped crystals (high pump and CR efficiencies) leading to high laser efficiency [14]. For PQS lasers, the microchip concept offers short output pulses due to the reduction of the cavity roundtrip time [13]. Indeed, the shortest (few ns-long or even sub-ns) pulses from a PQS oscillator at ~2 μm were reported in PQS Tm microchip lasers [15,16]. An important remark about microchip lasers is that they require a positive thermal lens of the active material to ensure the stabilization of the laser mode [14].

In the present work, we report on a detailed comparative investigation of the three tetragonal Tm:LiLnF$_4$ crystals (with Ln = Y, Gd, and Lu) for microchip lasers at ~1.91 μm and even beyond ~2 μm, including a comparison of their spectroscopic properties, parameters of the thermal lens and the laser performance.

2. Experimental

2.1 Studied crystals

The three LiLnF$_4$ crystals (with Ln = Y, Gd, and Lu) studied were grown by the Czochralski method using LiF, LnF_3 and TmF_3 (and HoF_3) reagents. The YLF and GLF crystals were doped with 8 at.% Tm^{3+}, and the LLF crystals - with 8 and 12 at.% Tm^{3+}. High doping levels are selected to provide efficient CR for Tm^{3+} ions and increase the pump absorption. In addition, one codoped 5.2 at.% Tm^{3+}, 0.5 at.% Ho^{3+}:YLF crystal was studied.

The Tm:LiLnF$_4$ crystals are tetragonal (space group C^6_{4h} - $I4_1/a$). For YLF, the lattice parameters are $a = b = 5.164$ Å, $c = 10.741$ Å. The as-grown bulks were oriented with the X-ray Laue technique. All laser elements were cut for light propagation along the ***a***-axis and polished to laser quality. They remained uncoated. Their dimensions as well as the Tm content are listed in Table 1. The Tm:LiLnF$_4$ crystals are optically uniaxial with the optical

Optical Materials EXPRESS

axis parallel to the ***c***-axis. Thus, for an *a*-cut crystal, two principal light polarizations are available, ***E*** || ***c*** (π) and ***E*** ⊥ ***c*** (σ). The refractive indices of YLF at ~1.91 μm are n_o = 1.443 and n_e = 1.465 (positive uniaxial).

Table 1. Parameters of the Studied Tm:Li*Ln*F$_4$ Crystals

Crystal	N_{RE}, 10^{20} cm^{-3}	*t*, mm	Aperture, mm^2	Abs, %*
8.0 at.% Tm:YLF	11.1	3.38	3.10(c) × 2.96	58
8.0 at.% Tm:GLF	10.6	2.70	3.11(c) × 3.40	45
8.0 at.% Tm:LLF	11.5	2.63	3.17(c) × 3.22	46
12.0 at.% Tm:LLF	17.2	3.54	3.15(c) × 2.75	76
5.2 at.% Tm, 0.5 at.% Ho:YLF	7.2 (Tm), 0.7 (Ho)	3.68	3.07(c) × 2.63	49

*Total pump absorption in a micro-laser diode-pumped at ~791 nm, defined as Abs = P_{abs}/P_{inc}.

2.2 Microchip-type set-up

The laser crystals were placed in a plano-plano laser cavity, Fig. 1(a). They were wrapped in indium foil and mounted in a Cu-holder water-cooled to 12 °C. The cooling was provided from all 4 lateral sides. The pump mirror (PM) was anti-reflection (AR)-coated for 0.78–1.0 μm and high-reflection (HR)-coated for 1.8–2.1 μm. A set of output couplers (OCs) with transmission T_{OC} = 0.2%, 0.5%, 3%, 5% and 10% in the 1.8–2.1 μm spectral range were used. Both mirrors were placed as close as possible to the laser crystal. The geometrical cavity length was equal to the crystal thickness, cf. Table 1. The crystal was pumped using a fiber-coupled (numerical aperture NA = 0.15, fiber core diameter: 105 μm) AlGaAs laser diode (diode #1) temperature-tuned to λ_p ~791 nm ($^3H_6 \rightarrow {}^3H_4$ transition of the Tm^{3+} ion, Fig. 1(b)). The pump radiation was unpolarized. The output from the diode was collimated and focused into the crystal through the PM with a lens assembly (1:1 reimaging ratio, 30 mm focal length). The radius of the pump beam was w_P = 50 μm and its Rayleigh length $2z_R$ = 1.0 mm (M^2 ~31 for the pump beam). The OCs were partially reflecting at λ_p (~45%), so the pumping was in two passes. The total pump absorption under lasing conditions is specified in Table 1.

Strictly speaking, a *monolithic* microchip laser requires that both dielectric cavity mirrors are directly deposited onto the surfaces of the active element (or a stack of the active element and a SA) [12]. In our case, we may talk about a microchip-type laser or a micro-laser that is a prerequisite for the further design of monolithic devices.

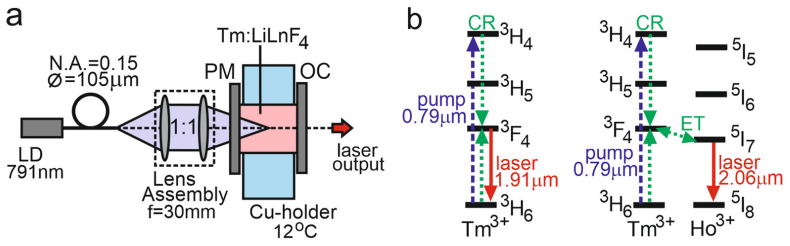

Fig. 1. (a) Scheme of the Tm:Li*Ln*F$_4$ micro-lasers: LD – laser diode, PM – pump mirror, OC – output coupler; (b) Scheme of the energy-levels of Tm^{3+} and Ho^{3+} ions showing the pump and laser transitions: CR – cross-relaxation, ET – energy-transfer.

2.3 Thermal lens measurements

The thermal lens was measured in the 8 at.% Tm:YLF, the 8 at.% Tm:GLF and the 12 at.% Tm:LLF crystals by analyzing the divergence of the output laser beam at various absorbed pump powers P_{abs}, see [17] for more details. A hemispherical laser cavity (radius of the OC: R_{OC} = 50 mm, T_{OC} = 5%, cavity length: 49 mm) was used. The crystal was pumped by a fiber-coupled (N.A. = 0.22, fiber core diameter: 200 μm) AlGaAs laser diode (diode #2) emitting unpolarized radiation at λ_p = 802 nm ($2z_R$ = 1.9 mm, M^2 ~59). The choice of this diode #2 is explained by better mode-matching of the pump (w_P = 100 μm) and laser (w_L = 95 ± 15 μm, depending on the thermal lens) beams in the crystal resulting in lower M^2 parameter of the output beam that is desirable for thermal lens evaluation.

Optical Materials EXPRESS

The optical (refractive) power of the thermal lens D (inverse of the focal length, $D = 1/f$) was calculated within the ray transfer matrix formalism [18]. The thermal lens was considered as an ideal thin astigmatic lens located at the center of the crystal. The radius of the output laser beam was measured by the optical knife method in the directions parallel and perpendicular to the laser polarization $\boldsymbol{E}$. For each measurement, the M^2 parameter of the laser beam was taken into account; it was in the 1.1-2 range for the studied P_{abs} (as measured in accordance with the ISO 11146-1 standard).

3. Spectroscopic properties

At first, we compared the transition cross-sections of the Tm^{3+} ions in the LiLnF$_4$ crystals relevant for diode-pumped microchip laser operation. The Tm^{3+} ions in the LiLnF$_4$ structure replace the "passive" Ln^{3+} ions in only one site (S_4 symmetry) with VIII-fold O^{2-}-coordination. The absorption cross-sections, σ_{abs}, for the $^3H_6 \rightarrow {}^3H_4$ and $^3H_6 \rightarrow {}^3F_4$ transitions of Tm^{3+} ions in a 8 at.% Tm:YLF crystal are shown in Fig. 2(a). They have been determined as $\sigma_{abs} = \alpha_{abs}/N_{Tm}$ where α_{abs} is the absorption coefficient; the absorption spectra were measured in polarized light ($\boldsymbol{E} \parallel \boldsymbol{c}$ and $\boldsymbol{E} \perp \boldsymbol{c}$) for $\boldsymbol{a}$-cut polished crystals. For the $^3H_6 \rightarrow {}^3H_4$ transition, σ_{abs} is higher for $\boldsymbol{E} \parallel \boldsymbol{c}$ (the maximum value is 0.79×10^{-20} cm^2 at 780.2 nm, the full width at half maximum, FWHM, of this peak is 7.7 nm). For $\boldsymbol{E} \perp \boldsymbol{c}$, the maximum σ_{abs} is 0.36×10^{-20} cm^2 at 790.6 nm, and FWHM = 16.4 nm. For the $^3H_6 \rightarrow {}^3F_4$ transition, the maximum $\sigma_{abs} = 1.21 \times 10^{-20}$ cm^2 is observed at 1681.6 nm for $\boldsymbol{E} \parallel \boldsymbol{c}$. The absorption properties of the Tm:YLF, Tm:GLF and Tm:LLF crystals are similar, see Fig. 2(b,c). Note the red-shift of the absorption of Tm^{3+} ions in GLF due to the larger difference of ionic radii of Tm^{3+} (0.994 Å) and Gd^{3+} (1.053 Å) as compared with Y^{3+} and Lu^{3+}.

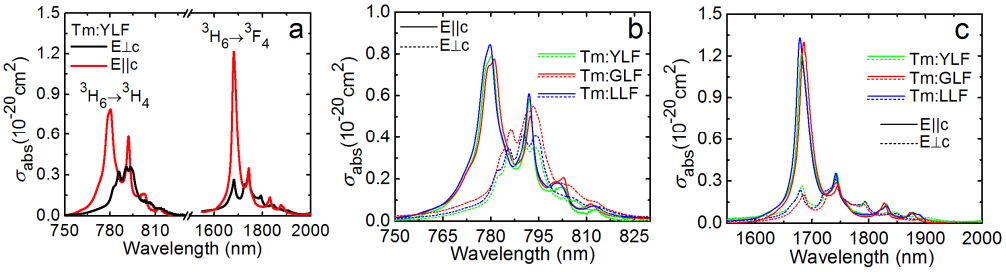

Fig. 2. Absorption cross-section, σ_{abs}, spectra for the $^3H_6 \rightarrow {}^3H_4$ and $^3H_6 \rightarrow {}^3F_4$ transitions of Tm^{3+} in 8 at.% Tm-doped YLF, GLF and LLF crystals for light polarizations $\boldsymbol{E} \perp \boldsymbol{c}$ and $\boldsymbol{E} \parallel \boldsymbol{c}$: (a) Tm:YLF crystal; (b) comparison for the $^3H_6 \rightarrow {}^3H_4$ transition; (c) comparison for the $^3H_6 \rightarrow {}^3F_4$ transition.

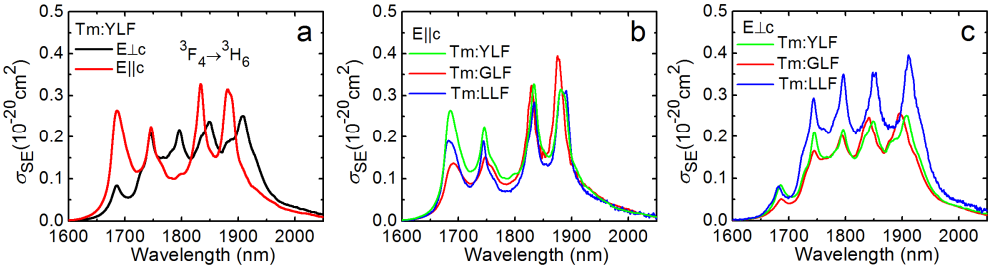

Fig. 3. Stimulated-emission (SE) cross-section, σ_{SE}, spectra for the $^3F_4 \rightarrow {}^3H_6$ transition of Tm^{3+} in 8 at.% Tm-doped YLF, GLF and LLF crystals for light polarizations $\boldsymbol{E} \perp \boldsymbol{c}$ and $\boldsymbol{E} \parallel \boldsymbol{c}$: (a) Tm:YLF crystal; (b) comparison for $\boldsymbol{E} \parallel \boldsymbol{c}$ polarization; (c) comparison for $\boldsymbol{E} \perp \boldsymbol{c}$ polarization.

The stimulated-emission (SE) cross-sections, σ_{SE}, for the $^3F_4 \rightarrow {}^3H_6$ transition of Tm^{3+}, see Fig. 1(b), derived by a combination of the reciprocity and Füchtbauer–Ladenburg (F-L)

Optical Materials EXPRESS

methods [19,20], are shown in Fig. 3. For Tm^{3+} in YLF, the maximum σ_{SE} corresponds to $\boldsymbol{E} \parallel \boldsymbol{c}$, 0.33×10^{-20} cm^2 at 1833.4 nm and it is lower for $\boldsymbol{E} \perp \boldsymbol{c}$, 0.25×10^{-20} cm^2 at 1907.7 nm, see Fig. 3(a). Tm^{3+} represents a quasi-three-level laser scheme [21]. In the spectral range where lasing occurs (long-wavelength part of the emission band), the σ_{SE} are higher for $\boldsymbol{E} \perp \boldsymbol{c}$ than for $\boldsymbol{E} \parallel \boldsymbol{c}$ for all the Tm:Li*Ln*F_4 crystals. The corresponding local peak in the SE cross-section spectra is located at ~1908 nm for Tm:YLF, 1900 nm for Tm:GLF and 1912 nm for Tm:LLF, see Fig. 3(c). A summary of the spectroscopic characteristics of the Tm:Li*Ln*F4 crystals is presented in Table 2.

Table 2. Comparison of the Spectroscopic Characteristics of the Tm:Li*Ln*F_4 Crystals

Crystal	σ_{abs}, 10^{-20} cm^2				σ_{SE}, 10^{-20} cm^2			
	$\boldsymbol{E} \perp \boldsymbol{c}$	λ_{abs} ($\Delta\lambda$), nm	$\boldsymbol{E} \parallel \boldsymbol{c}$	λ_{abs} ($\Delta\lambda$), nm	$\boldsymbol{E} \perp \boldsymbol{c}$	λ_{em}, nm	$\boldsymbol{E} \parallel \boldsymbol{c}$	λ_{em}, nm
Tm:LLF	0.41	790.2 (16.8)	0.84	779.8 (7.7)	0.39	1912	0.31	1881
Tm:YLF	0.36	790.6 (16.4)	0.79	780.2 (7.7)	0.25	1908	0.31	1881
Tm:GLF	0.55	793.5 (15.5)	0.77	781.1 (8.3)	0.26	1900	0.39	1875

*λ_{abs} and λ_{em} – peak absorption and emission wavelengths, respectively; $\Delta\lambda$ – FWHM of the absorption peak.

The selection of an ***a***-cut or ***c***-cut Tm:Li*Ln*F_4 crystal for microchip operation is based on both the spectroscopic and thermo-optic properties. According to the σ_{abs} spectra for the $^3H_6 \rightarrow {}^3H_4$ transition, ***a***-cut Tm:Li*Ln*F_4 crystals are more attractive in terms of higher pump efficiency. In addition, for this crystal cut, the anisotropy of the SE cross-sections of Tm^{3+} and the natural birefringence of the host promote the linearly polarized laser output.

Regarding the thermo-optic effects, the microchip lasers depend on the so-called thermal mode stabilization (thermal guiding) in a plano-plano laser cavity which is provided only by positive thermal lens. Characteristic of all these fluoride crystals and, in particular, of YLF is a negative thermo-optic coefficient, $dn_o/dT = -4.6 \times 10^{-6}$ K^{-1} and $dn_e/dT = -6.6 \times 10^{-6}$ K^{-1} [22]. Thus, positive thermal lens in this material is possible if only the negative contribution of dn/dT is cancelled by the positive contribution of the thermal expansion α. This can be expressed by the so-called "generalized" thermo-optic coefficient: $\Delta \approx dn/dT + (1 + \nu)(n - 1)\alpha$, where ν is the Poisson ratio ($\nu = 0.33$ for YLF) [23]. Specifically for YLF, $\alpha_a > \alpha_c$, namely 14.3×10^{-6} K^{-1} and 10.1×10^{-6} K^{-1}, respectively [22]. Thus, it is desirable to work with ***a***-cut Tm:Li*Ln*F_4 crystals which will provide stronger positive thermal lens due to the above-mentioned compensation ($\Delta \approx +3.8 \times 10^{-6}$ K^{-1}). For an ***a***-cut Tm:YLF crystal, the polarization ($\boldsymbol{E} \perp \boldsymbol{c}$) in the microchip laser will be selected also by the expected negative sign of the thermal lens for the $\boldsymbol{E} \parallel \boldsymbol{c}$ polarization [4].

4. Tm:Li*Ln*F_4 micro-lasers

4.1 Comparison of output performance

Laser operation in a plano-plano cavity was achieved will all four studied Tm:Li*Ln*F_4 crystals (cf. Table 1). In all cases, the laser output was linearly polarized, $\boldsymbol{E} \perp \boldsymbol{c}$ (σ).

The output characteristics for the 8 at.% Tm:YLF micro-laser are shown in Fig. 4(a). The best output performance corresponded to $T_{OC} = 5\%$. This laser generated 3.1 W at 1904 nm with a slope efficiency of $\eta = 72\%$ (with respect to P_{abs}). The laser threshold was at $P_{abs} = 0.24$ W and the optical-to-optical efficiency reached $\eta_{opt} = 38\%$ (with respect to the incident power). For $T_{OC} = 10\%$, the laser output was deteriorated which is attributed to increased upconversion losses related to higher inversion ratio β for Tm^{3+} ions. With the increase of T_{OC}, the laser emission wavelength shortened from 1991 to 2018 nm for $T_{OC} = 0.2\%$ to 1900-1916 nm for $T_{OC} = 10\%$, see Fig. 4(b). This behavior is due to the quasi-three-level nature of the Tm^{3+} emission and it is in agreement with the gain cross-section, $\sigma_g = \beta\sigma_{SE} - (1-\beta)\sigma_{abs}$, spectra when increasing the inversion ratio β, Fig. 4(c). The multi-peak spectral behavior is explained by the etalon effects resulting from the small separations of the optical elements in the microchip-type cavity. This effect is potentially interesting for THz generation. The emission at ~2 μm observed for low T_{OC} is due to the electron-phonon coupling (vibronic

Optical Materials EXPRESS

laser emission) [24]. The generation of σ-polarized output is in agreement with the dominance of $\sigma_g(\boldsymbol{E} \perp \boldsymbol{c})$ over $\sigma_g(\boldsymbol{E} \parallel \boldsymbol{c})$ at low inversion ratios, $\beta < 0.3$, Fig. 4(c), although the relation of the peak SE cross-sections is opposite, see Fig. 3(a).

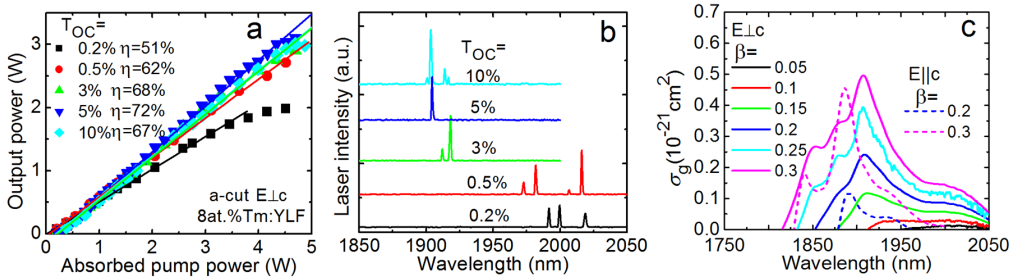

Fig. 4. Tm:YLF micro-laser: (a) input-output dependences, η – slope efficiency; (b) typical laser emission spectra at P_{abs} = 4.5 W; (c) gain cross-section, $\sigma_g = \beta\sigma_{SE} - (1-\beta)\sigma_{abs}$, spectra for Tm:YLF for light polarizations $\boldsymbol{E} \perp \boldsymbol{c}$ (σ) and $\boldsymbol{E} \parallel \boldsymbol{c}$ (π), β is the inversion ratio.

In Fig. 5(a), we compared the laser performance of all four studied Tm-doped crystals (Table 1) for the same T_{OC} = 5%. The Tm:GLF laser generated 1.87 W at 1902 nm with η = 65% and η_{opt} = 27%. The laser threshold was at P_{abs} = 0.29 W. The power scaling was limited by lower absorption and lower thermal fracture limit which is most probably due to a higher lattice distortion owing to the difference in ionic radii of Tm^{3+} and Gd^{3+}. The Tm:LLF laser with the 12 at.% Tm-doped crystal generated 2.65 W at 1916 nm with η = 52% and η_{opt} = 37%. The laser threshold was at P_{abs} = 0.46 W. For the LLF crystal with 8 at.% Tm doping, the output performance was inferior. For the same 5% OC, the emission wavelength shortened following the Tm:LLF – Tm:YLF – Tm:GLF series, Fig. 5(c), in agreement with the position of the long-wavelength local peak in the σ_{SE} spectra, as shown in Fig. 3(c). A summary of the output characteristics of the Tm:LiLnF$_4$ micro-lasers is presented in Table 3.

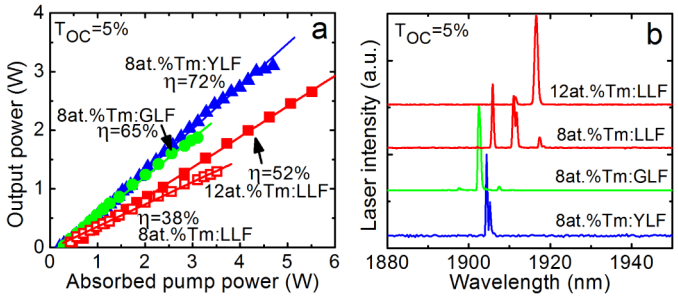

Fig. 5. Comparison of the (a) input-output characteristics and (b) typical laser emission spectra (at maximum P_{abs}) for Tm:YLF, Tm:GLF and Tm:LLF micro-lasers, η - slope efficiency.

Table 3. Comparison of the Output Characteristics of the Tm:LiLnF$_4$ Micro-Lasers

Crystal	P_{out}, W	λ_L, nm	η, %	P_{th}, W	η_{opt}, %
12.0 at.% Tm:LLF	2.65	1916	52	0.46	37
8.0 at.% Tm:YLF	3.10	1904	72	0.24	38
8.0 at.% Tm:GLF	1.87	1902	65	0.29	27

4.2 Micro-lasers beyond 2 μm

Laser operation beyond 2 μm with Tm-doped crystals is possible in two ways. One approach is the codoping with Ho^{3+} ions (keeping the Ho/Tm ratio low to minimize the upconversion mechanism) [25]. The Ho^{3+} ion emits above 2 μm according to the $^5I_7 \rightarrow {}^5I_8$ transition, and the excitation is provided by the energy-transfer (ET) $Tm^{3+}(^3F_4) \rightarrow Ho^{3+}$ ($^5I_7$), see Fig. 1(b). The results for the 5.2 at.% Tm, 0.5 at.% Ho:YLF crystal are shown in Fig. 6(a). The maximum output power from this laser reached 378 mW at 2065 nm corresponding to η =

Optical Materials EXPRESS

25% (T_{OC} = 3%). The laser threshold was at P_{abs} = 0.48 W and η_{opt} = 9%. The laser operated with $\boldsymbol{E} \perp \boldsymbol{c}$ polarization and the emission wavelength was weakly dependent on the OC, see Fig. 6(b), corresponding to a local maximum in the σ_{SE} spectra of the Ho^{3+} ions in YLF, Fig. 6(c). A thermal roll-over was observed for P_{abs} > 2 W attributed to a much stronger heating of the crystal related to upconversion [25,26] and finite ET probability. Indeed, the fractional heat loading, $\eta_h \approx 0.45$ for Tm,Ho:YLF [26].

The second approach to achieve laser operation with a Tm^{3+}-doped crystal beyond 2 μm is the so-called vibronic coupling [24,27]. For Tm^{3+} in YLF, the longest wavelength of the purely electronic $^3F_4 \rightarrow {}^3H_6$ transition is 1931 nm (it occurs between the lowest Stark sub-level of the $^3F_4$ excite-state, 5599 cm^{-1}, and the highest sub-level of the $^3H_6$ ground-state, 419 cm^{-1}) [28]. Longer emission wavelengths are attributed to a coupling of the electrons that participate in the electronic transition $^3F_4 \rightarrow {}^3H_6$ with various phonons of the host (electron-phonon or vibronic coupling). The relaxation of a Tm^{3+} ion excited to the $^3F_4$ state may lead to the excitation of a phonon and the emission of one photon with lower energy (longer wavelength) [27]. In Fig. 4(b), the emission at around 2 μm observed for low T_{OC} (0.2, 0.5%) has a vibronic nature and it is supported by very smooth and broad gain spectra for low inversion ratios β < 0.05 inherent to low outcoupling losses, Fig. 4(c).

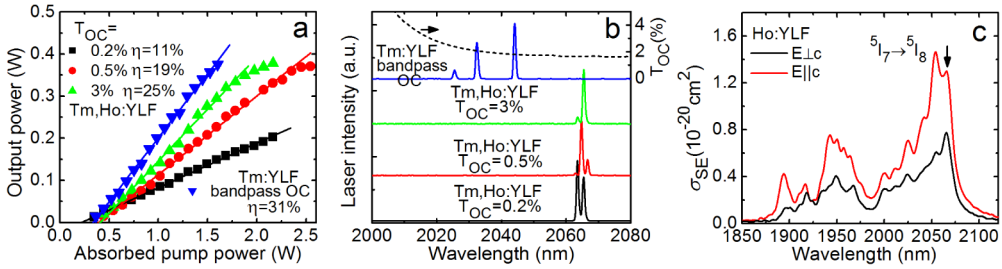

Fig. 6. (a) Input-output characteristics and (b) typical laser emission spectra (at maximum P_{abs}) for the "vibronic" Tm:YLF micro-laser with a "bandpass" OC and the Tm,Ho:YLF micro-laser with different OCs, η - slope efficiency; *dashed curve* – transmission spectrum of the "bandpass" OC; (c) σ_{SE} spectra for the $^5I_7 \rightarrow {}^5I_8$ transition of Ho^{3+} in YLF for light polarizations $\boldsymbol{E} \perp \boldsymbol{c}$ (σ) and $\boldsymbol{E} \parallel \boldsymbol{c}$ (π), *arrow* denotes the laser wavelength.

The vibronic operation at even longer wavelengths can be promoted by using a selective ("bandpass") OC [27], e.g. as in the present work. Such OC was specified for high transmission at 1.9–1.97 μm and T_{OC} = 1.6% at 2.05–2.20 μm (see the transmission spectrum in Fig. 6(a)). The results are shown in Fig. 6(a,b). The maximum output power reached 375 mW at 2026-2044 nm corresponding to η = 31% (i.e., better than the Tm,Ho:YLF micro-laser). The laser threshold was P_{abs} = 0.35 W and η_{opt} = 14%. The maximum phonon energy of YLF ν_{ph} is ~560 cm^{-1} [29] The observed emission lines are attributed to the coupling with the Raman-active modes occurring at ν_{ph} = 240-290 cm^{-1} and assigned as $A_{g(u)}$ and B_g [29].

5. Thermal lensing

The thermal lensing in Li$Ln$$F_4$ crystals has been extensively studied for the case of diode-pumped Nd:YLF laser rods [4,7]. It was shown that the thermal lens is positive for an ***a***-cut crystal and $\boldsymbol{E} \perp \boldsymbol{c}$ polarization. For Tm-doped YLF, only the information on the fractional heat load exists ($\eta_h \approx 0.36$) [1]. Thermal stress and end-bulging in Tm:YLF crystals were evaluated theoretically in [23]. In the present work, we characterize, for the first time, the thermal lens in diode-pumped ***a***-cut Tm:YLF, Tm:GLF and Tm:LLF crystals.

The results on the optical power of the thermal lens are shown in Fig. 7 and summarized in Table 4. These results correspond to the polarization and wavelength of the built lasers. For all studied crystals, the polarization was $\boldsymbol{E} \perp \boldsymbol{c}$ (σ) and the emission spectra were similar to those plotted in Fig. 5(b). The thermal lens is positive (focusing) for all Tm:Li$Ln$$F_4$ crystals. This finding is in agreement with the feasibility of microchip operation with these crystals,

Optical Materials EXPRESS

Fig. 5(a). The thermal lens shows an almost linear dependence of its optical power on P_{abs}, expressed by the so-called sensitivity factor, $M = dD/dP_{abs}$ [30]. The thermal lens in Tm:Li*Ln*F_4 is astigmatic, as its optical power is different for rays lying in different meridional planes and is confirmed by the ellipticity of the output laser beam. The principal meridional planes of the thermal lens A(B) correspond to the beam semiaxes and in our case they coincide with the directions along the ***a***- and ***c***-axes. This agrees with the theoretical modeling and is related to the anisotropy of the thermal expansion [23].

The thermal lens is weaker for Tm:YLF than for the other two fluoride crystals, M = 4.0 and 3.6 m^{-1}/W (for the meridional planes containing the directions $\parallel$ ***c*** and $\perp$ ***c***-axis, respectively). For Tm:LLF, it is slightly stronger, M = 4.3 ($\parallel$ ***c***) and 3.9 ($\perp$ ***c***) m^{-1}/W and for Tm:GLF, M = 5.6 ($\parallel$ ***c***) and 4.2 ($\perp$ ***c***) m^{-1}/W for the two principal meridional planes, respectively. The astigmatism of the thermal lens is defined as the difference of its refraction in the principal meridional planes [30]. The astigmatism degree, $S/M = |M_A - M_B|/M_{max}$ [30], equals 10%, 25% and 9% for Tm:YLF, Tm:GLF and Tm:LLF, respectively. Such a different thermo-optic behavior (stronger thermal lens with higher astigmatism) of the Tm:GLF crystal is attributed to a stronger distortion of its lattice with the incorporation of the Tm^{3+} ions. The thermal lens astigmatism in ***a***-cut tetragonal crystals is related to the net action of two effects: the photo-elastic effect and the stress-related component of end-bulging, both originating from the thermal stress in the crystal [31].

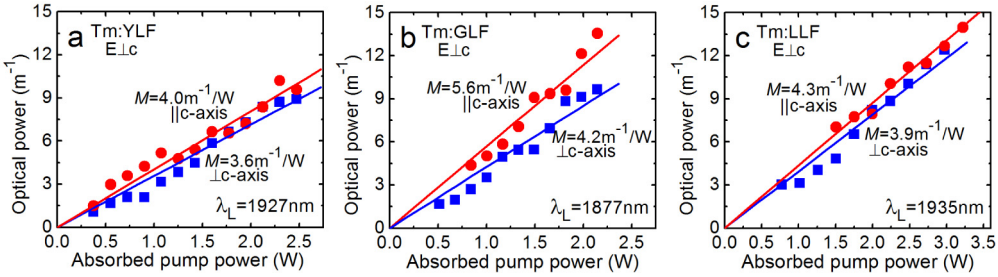

Fig. 7. Optical (refractive) power of the thermal lens vs. absorbed pump power in 8 at.% Tm:YLF (a), 8 at.% Tm:GLF (b) and 12 at.% Tm:LLF (c) crystals: pump wavelength, λ_p = 802 nm; pump spot radius, w_p = 100 μm, laser polarization, ***E*** $\perp$ ***c*** (σ): *symbols* – experimental data, *lines* – linear fits for the extraction of the sensitivity factor (M).

Table 4. Comparison of the Thermal Lens Parameters of the Tm:Li*Ln*F_4 Crystals (*a*-cut, *E* $\perp$ *c*)

Crystal	M, m^{-1}/W		S/M, %	λ_L, nm
	$\parallel$ ***c***	$\perp$ ***c***		
12.0 at.% Tm:LLF	4.3	3.9	9	1935
8.0 at.% Tm:YLF	4.0	3.6	10	1927
8.0 at.% Tm:GLF	5.6	4.2	25	1877

The sensitivity factor of the thermal lens in a diode-pumped crystal is represented as [30]:

$$M = \frac{\eta_h}{2\pi w_p^2 \kappa} \cdot \Delta, \qquad (1)$$

where κ is the thermal conductivity, 5.3 W/mK ($\parallel$ ***c***) and 7.2 W/mK ($\perp$ ***c***) for YLF [22]. In this formula, the pump beam is assumed to be "top-hat" [32]. Using the data for Tm:YLF, we calculate Δ = 4.4 and 4.0 × 10^{-6} K^{-1} ($\parallel$ ***c*** and $\perp$ ***c***, respectively) which agree with the value estimated above. The thermal lens in an ***a***-cut Tm:YLF crystal is ~3 times weaker than in an athermal N_g-cut monoclinic Tm:$KLu(WO_4)_2$ (Tm:KLuW) crystal previously studied under the same pump conditions (M = 12.9 and 8.1 m^{-1}/W along the N_p and N_m axes, respectively, or, equivalently, Δ = 8.8 and 5.5 × 10^{-6} K^{-1}, so S/M = 37%) [14]. The weaker thermal lens in

Optical Materials EXPRESS

Tm:YLF is attributed to the higher thermal conductivity and lower Δ in YLF due to the better compensation of the counteraction of dn/dT and α. In addition, Tm:YLF provides lower astigmatism of the thermal lens.

It is worth noting that the thermal lens experiment was performed using the diode #2 (λ_p = 802 nm, w_P = 100 μm) targeting a better precision of the evaluated optical power D, while in the microchip laser experiment – using the diode #1 (λ_p = 791 nm, w_P = 50 μm) the target was to achieve a higher slope efficiency. This difference does not influence the sign of the thermal lens, the relation of M-factors for the two meridional planes and the astigmatism degree S/M. The absolute value of M will vary mostly due to the difference in w_P. This effect can be accounted with Eq. (1).

The nearly spherical thermal lens in Tm:YLF (S/M = 10%) is responsible for the generation of an almost circular output laser beam in the corresponding micro-laser with a measured $M^2_{x,y} < 1.05$ at the maximum studied P_{abs}.

The thermal stress is the reason for thermal fracture of the laser crystals. For diode-end-pumped crystals (plane stress approximation), the fracture occurs when the tangential (hoop) stress σ_θ at the crystal periphery exceeds the tensile stress σ_{TS} (~40 MPa for YLF) [23]. By using the previously reported method for stress calculations in tetragonal crystals [23], we determined the "stress sensitivity factor", $M_\sigma = d\sigma_\theta/dP_{abs}$ as 4.4 MPa/W that corresponds to the maximum stress of ~22 MPa in the Tm:YLF crystal (below σ_{TS}). Indeed, no thermal fracture of Tm:YLF was observed but the power scaling was limited by the thermal roll-over at high P_{abs}, Fig. 4(a). Thus, we attribute this roll-over to the temperature-dependence of the spectroscopic and thermal parameters of the crystal which was strongly heated due to localized heat loading under tight focusing of the pump beam.

6. Discussion

The very high slope efficiency achieved with the Tm:YLF micro-laser (T_{OC} = 5%) is a consequence of the efficient CR for adjacent Tm^{3+} ions under high doping (8 at.%), the good mode-matching conditions when pumping with a small pump spot size and relatively low losses in the laser crystal (including low upconversion loss for small T_{OC}). The slope efficiency of a Tm laser can be represented as [33]:

$$\eta = \eta_{St} \cdot \eta_q \cdot \eta_{mode} \cdot \eta_{OC}, \quad (2)$$

where the four terms denote the Stokes, quantum, mode-matching and outcoupling efficiencies, respectively. η_{St} is defined as λ_p/λ_L (λ_L – laser wavelength) and equals in our case, η_{St} = 0.415. For 8 at.% Tm-doped YLF, $\eta_q > 1.96$ [1] due to an efficient CR. The mode overlap in the considered laser can be calculated with the determined parameters of the thermal lens. One needs to take into account the dependence of the M-factor of the thermal lens on w_p, see Eq. (1), so $M' = M \cdot (w_p/w_p')^2$ where M' is a sensitivity factor corresponding to a different pump spot size w_p'. Then, we obtain w_L = 62 ± 5 μm with η_{mode} ≈0.94. The η_{OC} is expressed as $\ln[1-T_{OC}]/\ln[(1-T_{OC})\cdot(1-L)]$ where L is the roundtrip passive loss that can be estimated from the Caird plot [34], i.e. plotting the inverse of the slope efficiency vs. the inverse of the output coupling, $1/\eta = 1/\eta_0 + (L/\eta_0)\cdot(1/T_{OC})$. From the data presented in Fig. 4(a) with the exception of the T_{OC} = 10% OC where the upconversion effects are not negligible, we estimate the loss coefficient as δ ~0.0011 cm^{-1} ($L < 1 \times 10^{-3}$). As a result, η_{OC} > 0.99. Finally, the theoretical value for η is 75% in good agreement with the experimental value (72%).

The previous work on Tm:YLF microchip laser focused on single-longitudinal-mode (SLM) operation and thus power scaling was not targeted [35]. Microchip lasers based on Tm:GLF and Tm:LLF have never been reported previously. In the present study, we report on efficient multi-watt microchip operation with all three Tm:Li$Ln$$F_4$ crystals. As compared with a previous report on a Tm:KLuW microchip laser [14], we achieved, with Tm:YLF, a similar output power (~3 W) and much higher slope efficiency (78% vs. 50.4%). There are multiple reports on Tm,Ho:YLF microchip lasers operating both in the SLM and multi-mode regimes,

Optical Materials EXPRESS

see e.g [36]. The authors in [36], achieved ~1 W with η = 54% using a 6 at.% Tm, 0.4 at.% Ho:YLF crystal in a monolithic design. These results are better than those in the present work most probably due to the non-optimum Ho/Tm codoping ratio.

The vibronic laser operation with Tm:YLF extends recent findings in this field with other fluoride (Tm:BaY_2F_8) [24] and oxide (Tm:KLuW) [27] Raman-active crystals. Further improvement of the laser output and efficiency of vibronic Tm:Li*Ln*F_4 lasers is expected by using high Tm doping levels (8-12 at.%) and proper laser mirrors. In this way, we expect laser emission at ~2.05-2.1 μm.

Further power scaling of Tm:Li*Ln*F_4 microchip lasers is possible by optimizing the doping level (in our case for 8 at.% Tm doping of YLF, a clear effect of upconversion loss was detected for T_{OC} = 10%, see Fig. 4(a)) and the pump spot size. In this way the temperature and stress fields in the laser crystal will be compromised. Consequently, the slope efficiency of the Tm:GLF and Tm:LLF microchip lasers may be enhanced up to ~70%.

The performed study of the thermal lens in tetragonal Tm:Li*Ln*F_4 crystals indicates the compensation of various effects (d*n*/d*T*, end-bulging related to the thermal expansion and the photo-elastic effect) leading to a positive thermal lens, a situation not reached for cubic (higher symmetry) fluorides such as CaF_2 or SrF_2 [37]. A similar effect is expected for the monoclinic (lower symmetry) Tm:BaY_2F_8 crystal [24] which has not been exploited for microchip lasers yet. Further work will focus also on direct measurements of the d*n*/d*T* coefficients for the Li*Ln*F_4 crystals.

7. Conclusion

Tetragonal Tm:Li*Ln*F_4 crystals are attractive for highly-efficient microchip lasers, diode-pumped at ~791 nm and operating at ~1.91 μm, due to the combination of a high Tm doping level (and, hence, efficient CR), their spectroscopic properties and weak, positive and low-astigmatic thermal lensing (for ***a***-cut crystals). The relatively high thermal conductivity and acceptable tensile stress allows for power scaling to multi-watt output using very compact (few mm-long) devices. In this way, an ***a***-cut 8 at.% Tm:YLF micro-laser generated 3.1 W at 1904 nm with a slope efficiency of η = 72% and a laser threshold as low as 0.24 W while ~2 W output power was achieved with both Tm:GLF and Tm:LLF. The possibility to operate such laser oscillators beyond ~2 μm (2000-2044 nm) is demonstrated with a Tm:YLF crystal using the vibronic coupling and compared to the conventional Tm,Ho-codoping scheme. The extension of the microchip concept to other anisotropic fluorides (Tm:BaY_2F_8) seems very promising.

Funding

This work has received funding from the European Union's Horizon 2020 research and innovation programme under the Marie Skłodowska-Curie grant agreement No 657630. P.L. acknowledges financial support from the Government of the Russian Federation (Grant 074-U01) through ITMO Post-Doctoral Fellowship scheme.